Realistic Litz Wire Characterization using Fast Numerical Simulations

Richard Y. Zhang, Jacob K. White,
and John G. Kassakian
Electrical Engineering & Computer Science
Massachusetts Institute of Technology
Cambridge, MA 02139, USA
{ryz, white, jgk}@mit.edu

Charles R. Sullivan
Thayer School of Engineering at Dartmouth
Hanover, NH 03755, USA
charles.r.sullivan@dartmouth.edu

Abstract—The losses of realistic litz wires are characterized while explicitly accounting for their construction, using a procedure that computes the current-driven and magnetic-field–driven copper losses using fast numerical simulations. We present a case study that examines loss variation in one- and two-level litz wires as a function of twisting pitch, over a wide range of values and in small increments. Experimental confirmation is presented for predictions made by numerical simulations. Results confirm the capability and efficiency of numerical methods to provide valuable insights into the realistic construction of litz wire.

I. INTRODUCTION

The efficiency of high-frequency power magnetic components can often be improved by the use of litz wire, which is constructed from small insulated strands, woven or twisted to distribute the current density over the entire cross-sectional area of the wire, as shown in Fig. 1.

The decision to use litz wire over equivalent solid wire comes down to the tradeoff between the loss reductions offered and the associated increase in costs [1]. A significant portion of the cost of litz wire come from its construction, but even simply twisted strands may provide satisfactory efficiency benefits. In fact, it was shown that even twisted strands of uninsulated copper can provide significant loss reductions over solid wire [2].

The primary challenge in optimizing litz wire construction, however, stems from the difficulty in quantifying the achievable loss reductions. Experimental characterization procedures, like those described in [3], require intricate test equipment, as well as many litz wire samples to be manufactured and prepared over a meaningful range of construction parameters. On the other hand, general-purpose three-dimensional numerical simulations can often be very computationally expensive, requiring the use of "high-throughput computing [with] distributed computer resources" [4]. For these reasons, existing litz wire optimizations have largely focused on balancing the number of strands, assuming ideal litz wire construction that successfully equalizes the current through each strand [1], [5], [6].

In this paper, we describe a computational procedure to characterize the losses in realistic litz wire constructions, with the aid of a fast numerical simulation tool recently presented
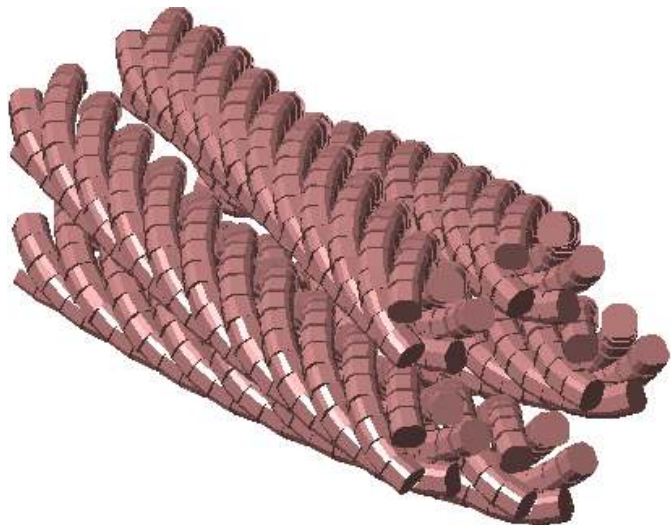

Figure 1: The circular litz wire construction recursively twists strands of wire into bundles, and bundles of wire into larger bundles, resulting in a pattern that allows each strand to traverse all radial and azimuthal positions in the wire cross-section.

in [7]. Existing theory, which lies at the heart of prior litz wire optimizations, computes copper losses as the sum of two loss components, one driven by the net current flow, and the other driven by the external magnetic field [8]. We extend this approach by simulating both loss mechanisms numerically, for realistic models of litz wire that include the underlying construction details. Exploiting the high speed of the procedure, we swept the pitches of the wires over a large range of values, revealing a number of insights in the construction of the wire. The predictions of the characterization are confirmed with experimental measurements.

II. BACKGROUND

A. Copper loss theory

Within the field of power electronics, it is common to refer to high-frequency conductor losses as consisting of two approximately orthogonal components, respectively due to the

skin effect and the *proximity effect* [8], as in,

$$P_{tot}(f) = P_{skin}(f) + P_{prox}(f). \tag{1}$$

The former term is generally reserved for the eddy losses that are self-induced. The latter term generally refers to the eddy losses induced by external magnetic fields, for example the stray magnetic fields from nearby turns, or from the magnetic core. Both terms include eddy currents that circulate within strands and eddy currents that circulate among different strands. By this description, we can write the components as ultimately driven respectively by the net current magnitude I, and the external magnetic field magnitude $|H|$, as in,

$$P_{skin}(f) = F(f)I^2 R_{dc}, \quad P_{prox}(f) = G(f)|H|^2, \tag{2}$$

where F and G are important wire parameters that fully describe the frequency dependence of the wire material, defined over a unit length and for either rms or peak values of I and H. This simple equation is the basic building block for copper loss equations in all kinds of devices constructed from wound conductors. The interested reader is referred to [8]–[10] for details on its derivation and application.

The two geometry factors, F and G, are important parameters that characterize a particular wire material and construction. The F factor is a unit-less quantity also known as R_{ac}/R_{dc}, the a.c. / d.c. resistance ratio. It measures the frequency dependence of the resistance in a single isolated wire—in a very large loop, or in the theoretical limit, stretching from infinity to infinity. The G factor is a magnetic diffusion loss term, with units of watts per A/m squared per unit length, and measures the losses induced in the wire material when it is exposed to a unit, uniform magnetic field excitation in a transverse direction.

Exact solutions for F in single-stranded round wire are well-known, and also for G if it is assumed that the external magnetic field is transverse, homogenous and uniform over the wire [8], [11]. These solutions lead to approximate closed-form expressions for F and G in bundled, multi-stranded wire like litz wire, by assuming that each strand carries the same current distribution within the bundle. If the wires are wound into a winding, perhaps within the window of a magnetic core, then the entire winding cross-section can be considered as a region of uniform current density, and similar closed-form expressions can be derived [5], [9].

The closed-form solutions have provided power electronics designers with valuable insight into the underlying physics of copper loss, and have also been extensively used in optimization for picking the right wire for each application. However, very little is revealed on how the wire should be twisted to achieve the constant current density that had simply been assumed during the derivation of these equations. Moreover, where a litz wire specimen deviates from ideal construction—by mistake or by design—these equations lose a lot of their predictive power, and the designer must fall back on experimental techniques.
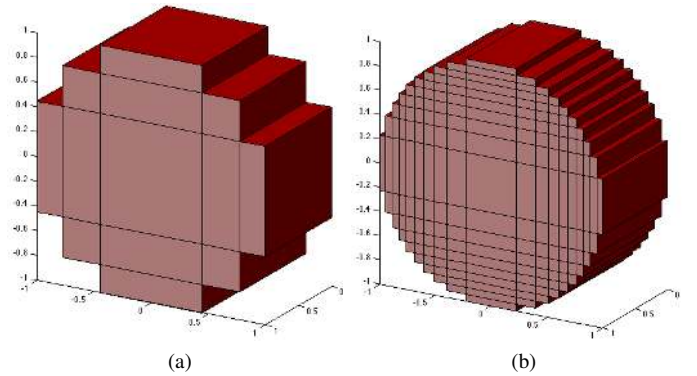

Figure 2: The filament discretization in the Partial Element Equivalent Circuit method. Discretization parameter of (a) 3; and (b) 10.

B. Fast numerical simulations

Numerical simulations can overcome many of the deficiencies in analytical equations, and be used to analyze the impact of non-ideal construction. However, this comes at a cost of significantly increased computation, and care must be taken to chose the most computationally efficient numerical method for the problem at hand.

The simulations in this paper were performed using the tool presented in [7], based upon an integral formulation of Maxwell's equations often known as the Partial Element Equivalent Circuit (PEEC) method [12], [13]. In essence, the PEEC method maps the electromagnetic problem into an equivalent circuit problem, by subdividing the conductive volume of an electromagnetic problem along its length and cross-section into current-carrying filaments, as shown in Fig. 2, and allowing the filaments to interact through self- and mutual-inductances [12], [14]. The method has found extensive use in the analysis of microelectronics and interconnects [13], [15]. Our PEEC implementation is similar to FastHenry [13], but with a number of optimizations in speed and accuracy specific to wire-based problems and magnetic field excitations [7].

The PEEC method derives its computation efficiency by restricting volumetric meshing only to the current-carrying conductive material, while implicitly accounting for the presence of the surrounding free-space. This typically results in 10-100 times reduction in the number of unknowns to be solved (e.g., see a comparison in [16]). The method is particularly efficient for power applications, because conductors, such as the individual strands in a bundle of litz wire, are usually carefully sized to be on the same order of magnitude as the skin depth. Restricting analysis frequencies to only those with reasonable copper loss allows us to use a relatively coarse mesh in the conductor without sacrificing accuracy.

We illustrate the accuracy and speed of the method for litz wire by benchmarking the simulation accuracy and timing against the fineness of the conductor meshing. The benchmark problem is to predict the F factor of a single-strand of AWG 38 wire, which has a well-known exact solution [11]. The
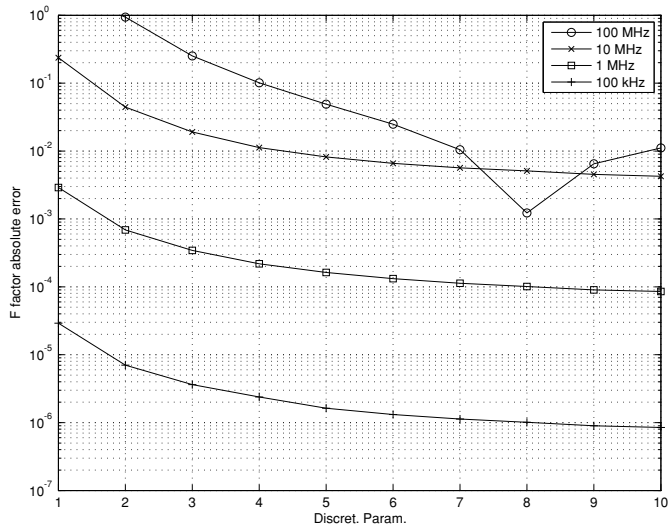
(a)
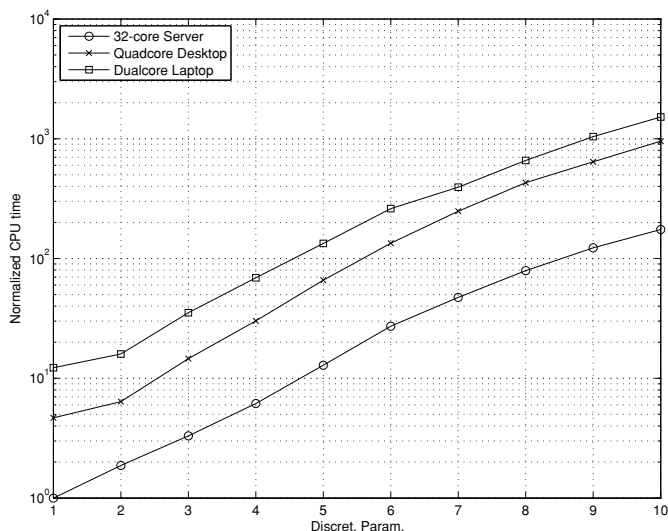
(b)

Figure 3: (a) F factor absolute error and (b) normalized simulation times for various levels of discretization. Note that since $F \approx 1$, its absolute error is in the same order of magnitude as the relative error. The simulation is for a single-strand of AWG 38 wire. The strand radius matches its skin depth at 1.75 MHz.

wire has a diameter of 0.101 mm and the skin depth matches the wire radius at 1.75 MHz. Lengthwise, the wire is divided into at least 20 segments for straight sections, and at least 12 segments per pitch length for curved sections. The cross-sectional meshes are illustrated in Fig. 2, where the grid is generated using a quadratic rule, and the "discretization parameter" is defined to be the number of elements along the radius of the circular cross-section, including the center element. Rectangular, brick-shaped elements were used in order to maximize computation speed [7]. Three computer platforms were tested, a dual-core 2.1 GHz laptop, a quad-core

2.5 GHz desktop workstation, and a dual-processor, 32-core 3 GHz computation server.

As shown in Fig. 3, the prediction error decreases logarithmically with fineness of discretization, but the simulation time also increases logarithmically. If an accurate prediction were desired at 100 MHz, or even 10 MHz, then the computation burden is quite considerable. However, a litz wire bundle constructed from AWG 38 wire is recommended for only 50 kHz - 100 kHz [17], and even then, only for low-cost, high-loss designs within this frequency range according to optimization techniques such as [1], [5]. Restricting the frequency sweep to 1 MHz, even a discretization level of 2, with just five elements per cross-section, is adequate to achieve a prediction error below 0.1%. Reducing discretization from 7 to 2 results in a 50-100 times speedup in all three tested platforms in Fig. 3b. To put this into perspective, solving the benchmark problem discretized to level 2 on the dual-core laptop was 4-5 times faster than solving the same problem discretized to level 7 on the 32-core computation server. To balance the trade-off between speed and accuracy, all remaining computations in this paper were performed with the discretization level set to 3.

III. NUMERICAL CHARACTERIZATION PROCEDURE

In this paper, we aim to complement—rather than to replace—the copper loss theory in Section II-A, by computing the F and G factors numerically for litz wire of realistic constructions. The objective is to allow existing design rules and optimization routines based on (2) for round, solid conductors (and/or the idealized litz wire) to be extended to include realistic litz wire without significant modifications. Furthermore, if a range of F and G factors are computed for many different constructions of litz wire, then the litz wire construction may be included in the optimization and design as an additional degree of freedom.

To limit the scope of this paper, we will focus our attention on litz wire with circular cross-sections. We note that the techniques presented are broadly applicable litz wire of all constructions; for example, litz wire with square cross-sections were analyzed and experimentally confirmed in [7].

A. Litz wire construction and modeling

Round litz wires are wound by recursively twisting bundles of strands together in multiple levels. At the lowest, innermost level are a small number of thin strands, which are twisted such that the path of each strand traces a helix. The axial distance traveled for one full rotation is known as the helical *pitch* of the twist. The twisting is then repeated recursively on the bundles to form a multilevel-level twisted wire structure, as previously shown in Fig. 1.

It is easy to see that the multilevel helical structure fits the definition of a litz wire, because each strand of wire at the lowest level is allowed to occupy all radial and azimuthal positions in the overall bundle. Consequently, every strand is forced to carry the same amount of current, and the constant-current density objective is achieved over the bundle. Note
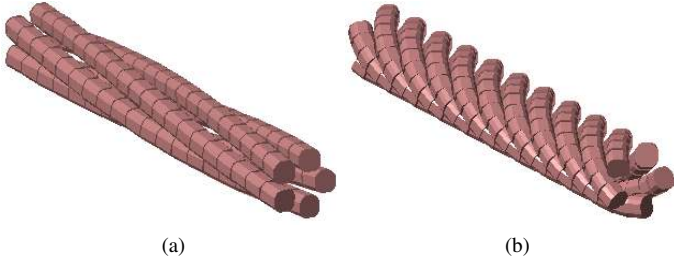
Figure 4: Five strands of AWG 38 wire twisted into: (a) 2 twists / cm; (b) 10 twists / cm. The strand insulation is hidden.

that the simply twisted wire with one level of twisting admits azimuthal, but not radial transposition, so would not meet a strict definition of true litz wire.

The mathematical model for the construction described above begins with a set of n evenly-spaced helical paths, whose center axis traces the path for the overall wire bundle. These paths can be converted into solid conductors by tracing a circular cross-section along their lengths. Alternatively, each helical path can be taken as the center axis for a smaller set of m helical paths, resulting in a two-level, $n \times m$ helical construction. At each individual level, all n paths share the same helical radius R and pitch P, which are interdependent if we assume that the wires are packed together with their insulation touching. Using trigonometry and multivariate calculus, it can be shown that the distance between neighboring helical paths is

$$D = \sqrt{2R^2 - 2R^2 \cos \psi + P^2(\psi - \phi)^2}, \qquad (3)$$

where ψ is the minimized helical phase difference, given as the solution to

$$R^2 \sin \psi + P^2(\psi - \phi) = 0, \qquad (4)$$

with $\phi = 2\pi/n$. The distance, D, will be minimized until the neighboring strands or bundles touch. This means that for a one-level bundle, D is set to the diameter of the constituent strands plus insulation, and for a specified pitch P, the value for R is found by solving (3). Similarly, for a multilevel bundle, D is set to the diameter of the bundle one level below, and R is found accordingly. Implementing this relationship between D and P allows the wire pitch to be set arbitrarily while maintaining tight contact between all neighboring strands.

B. Characterization

For brevity, we present a relatively high level discussion in this section, while bearing in mind that the electromagnetic problem has already been mapped to an equivalent circuit problem using the Partial Element Equivalent Circuit method. The reader is referred to [7], [12], [13] for implementation details. The full program and source code may be found at [18].

We begin with a straight segment model of the wire, with a length given by its real-life application; examples are shown in Fig. 4. In effect, this assumes that the current return path is at infinity, as if the segment of wire were a part of a larger loop of wire stretching from infinity to infinity. This simulation is faster to perform than one where a finite return path is explicitly modeled, and we have found it to give largely identical results.

The F factor, or the a.c. / d.c. ratio, is computed using standard impedance extraction techniques [13], [14]. First, the frequency-dependent resistance is obtained by placing a sinusoidal voltage across the segment within the equivalent circuit, and the net current flow is computed. Dividing through by the d.c. resistance yields the F factor.

The G factor, or the proximity effect factor, is obtained by exposing the segment model to a time-varying magnetic field over its volume, with its peak magnitude normalized to 1 A/m. By Faraday's law, this induces a voltage around each loop of current,

$$V_{loop} = \frac{\mu_0}{l} \int_S \mathbf{H} \cdot \hat{n} dA, \qquad (5)$$

where l is the length of the loop, S is the area of the loop, and $\hat{n}$ is the normal vector. If mesh analysis is used to solve the equivalent circuit, then we may iterate over each mesh loop and compute its induced voltage. The current distribution is computed by solving the equivalent circuit problem, and the power loss is computed by summing $i^2 R$ over each resistor. The G factor is then given as the total loss, divided by the length of the conductor.

IV. CASE STUDY

In this section, we provide a concrete case study, based on the procedures described above, in order to illustrate the capability of method, and to reveal some insights into the construction of litz wire. As previously summarized, the design degrees of freedom for the twisted, helical construction of litz wire are:

1) Strand diameter and insulation thickness,
2) Number of strands or bundles at each level, and
3) Helical pitch at each level, which may be either clock-wise or counter-clockwise.

Due to space constraints, we focus our analysis on the third degree of freedom, which is the helical pitch. As there already exists a large body of literature on the optimization for the first degree of freedom, we fix our analysis below to AWG 38 gauge magnetic wire, with diameters of 101 μm and insulation thicknesses of around 15 μm. The number of strands at each level is set to 5, and the length of the wire segment to 2 cm.

A. One-Level Sweeps

We begin with one level of twisting. Figure 5 shows a sweep of the total resistance and the F factor, with respect to frequency and the number of twists in the wire segment. It is immediately apparent that increasing the number of twists increases the d.c. resistance, thereby offsetting the benefits
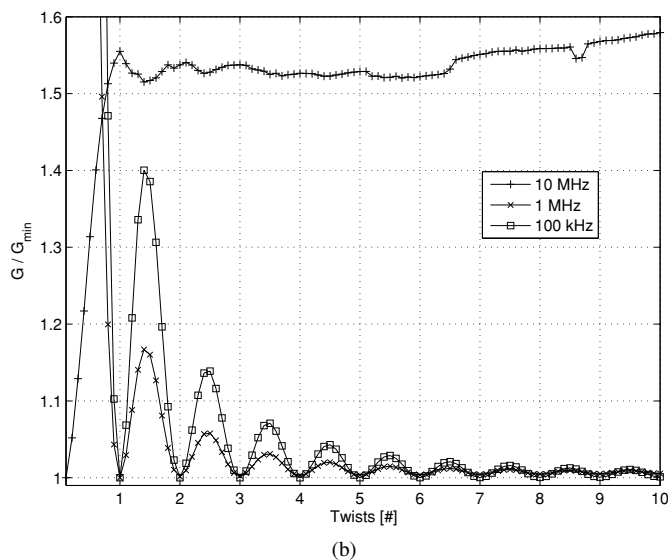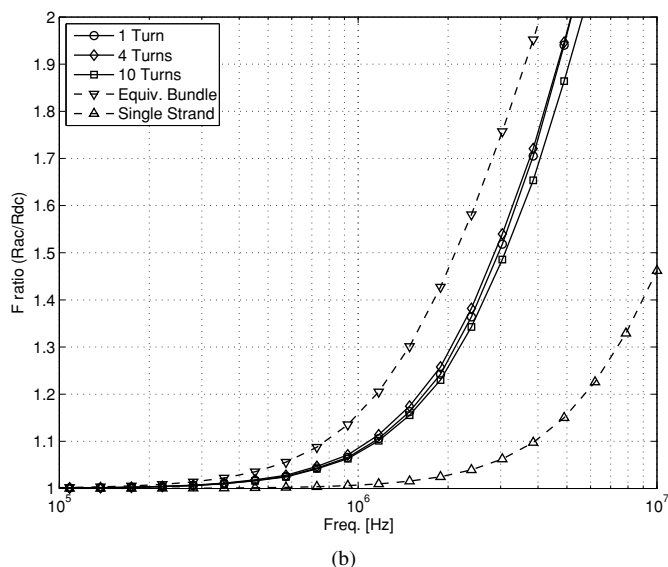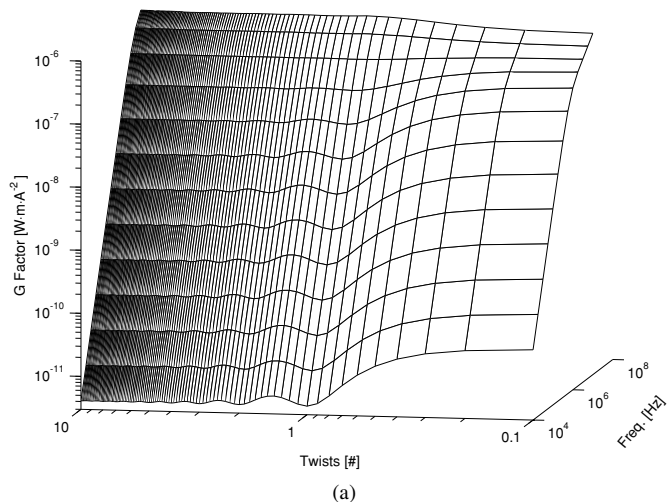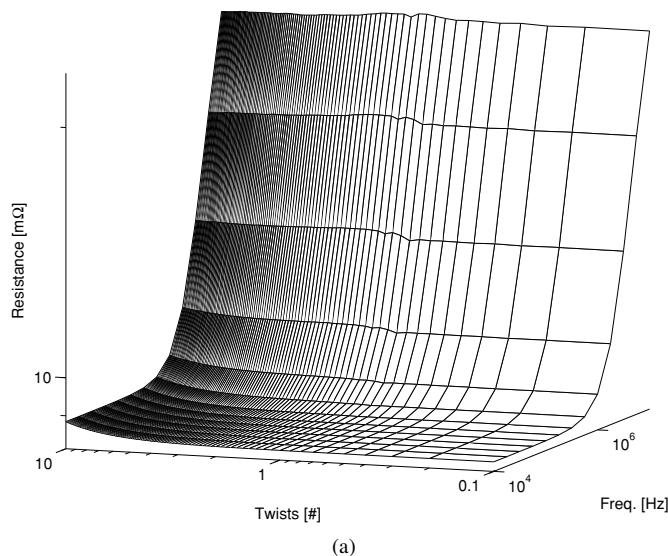
(a)

(b)

Figure 5: Five-stranded twisted wire: (a) Resistance; (b) F factor. Frequency from 10 kHz to 10 MHz. Number of twists from 0.25 to 10, in steps of 0.25 and 0.5.

(a)

(b)

Figure 6: Five-stranded twisted wire proximity effect G factor: (a) Surface plot; (b) Normalized to the minimum at each frequency. Frequency from 10 kHz to 100 MHz. Number of twists from 0.1 to 10, in steps of 0.1.

in the improvements of the F factor. As discussed in Section II-A, a one-level construction does not benefit from radial transposition, and so in isolation, its losses do not significantly decrease with increasing number of twists.

However, twisting mitigates proximity effect loss, as shown in Fig. 6. At 10 kHz, this reduction is a dramatic 90% when compared to the untwisted wire, but the benefits erode away with increasing frequency. These results are explained by noting that when a multi-stranded wire is placed in a magnetic field, two modes of eddy current flow are induced:

- The inter-strand eddies that circulate from strand to strand, which dominate loss at lower frequencies; and
- The intra-strand eddies that circulate within the body of each strand, which dominate at higher frequencies.

The azimuthal transposition afforded by a twisting construction allows the flux linkages associated with the inter-strand eddies to interact, and to perfectly cancel when there is an integer number of twists in the magnetic field. This leaves only the much smaller, intra-strand eddy currents to incur loss. However, the strategy becomes ineffective when the intra-strand eddies begin to dominate, particularly at higher frequencies. In these cases, losses are mitigated by minimizing the amount of conductor exposed transverse to the magnetic field.

B. Two-level twisted five-strands

We then consider the two-level, 5×5 structure with 25 strands. Here, the definition of the inner pitch demands particular attention, given it could be either:
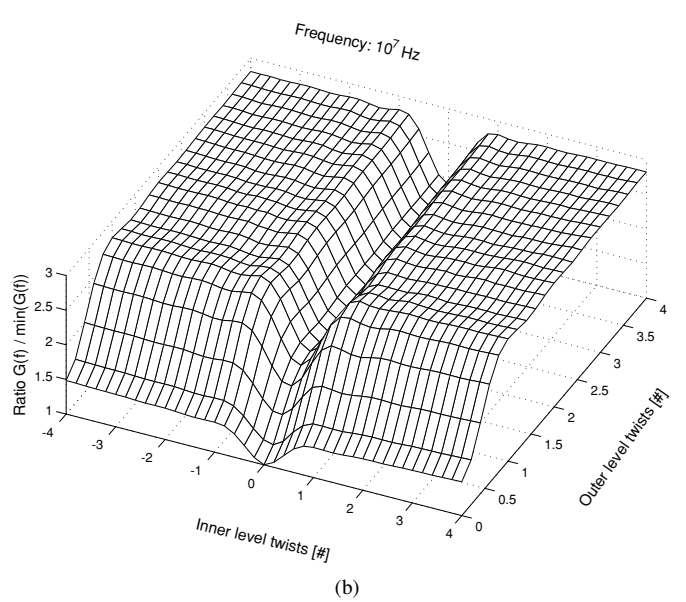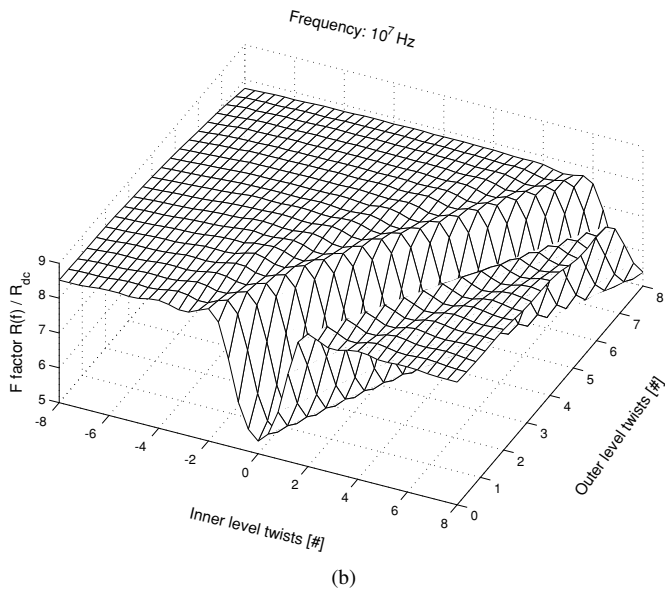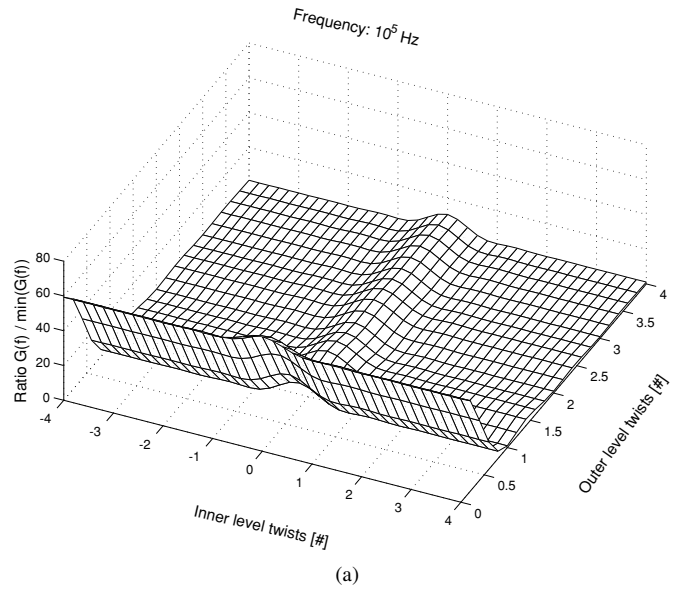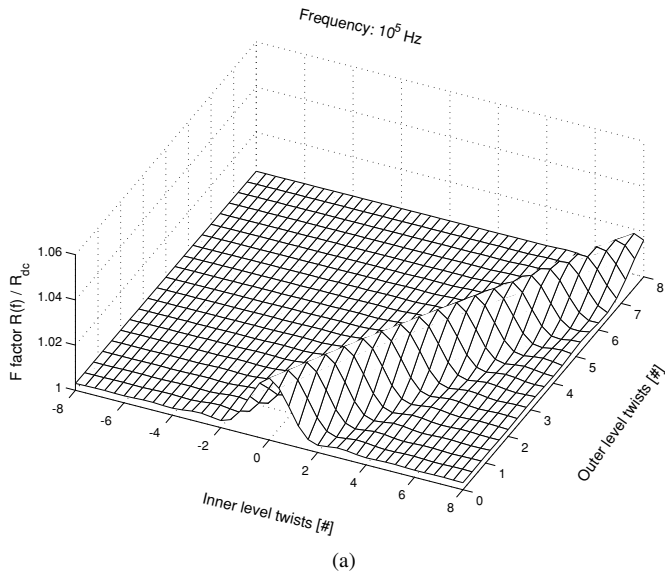
(a)

(b)

Figure 7: Two-level litz wire F factor sweep over inner level and outer level pitch, in steps of 0.2 twists: (a) $f = 100$ kHz; (b) $f = 10$ MHz.

1) The initial pitch before the twisting, defined using the second level as reference frame; or
2) The final pitch after the second level is constructed, defined relative to the global coordinates.

The figure labels take on the second definition, although both definitions will play a role in the discussion below. Additionally, we denote counter-clockwise number twists with a positive number, and clockwise twists with a negative number.

Figure 7 shows a sweep in the F factor at two frequencies, 100 kHz and 10 MHz. For each constituent inner level bundle, the external magnetic field it experiences is due to neighboring bundles. This external magnetic field flows normal to the helical path of the outer level. Consequently, high losses occur

(a)

(b)

Figure 8: Two-level litz wire G factor sweep over inner level and outer level pitch, in steps of 0.2 twists: (a) $f = 100$ kHz; (b) $f = 10$ MHz. The z-axis is normalized against the minimum value of G over all sweeps for that frequency.

where the inner level has zero twists *relative to the outer level*, corresponding to definition 1 from above. This forms a diagonal along definition 2, where inner pitch is equal to outer pitch. Effectively, these wires behave like one-level, 25-strand wires, rather than two-level, 5×5 wires. The main diagonal is accompanied by troughs, spaced integer number of twists away in either direction. These are cases where the inner level has an integer number of twists relative to the outer level, such that the internal proximity effects are minimized.

Figure 8 shows the same sweep for the G factor. With the external magnetic fields now uniform along the global

coordinates, corresponding to definition. The high loss lines of zero twist now occur along the axes, *relative to the global coordinates*. Again, an integer number of twists gives the lowest loss at 100 kHz, mitigating proximity losses by a factor of up to 60. This trend is largely reversed at high frequencies due to the same reasons as in the one-level case.

C. Summary

The twisting construction at each level mitigates that bundle's losses due to external magnetic fields, without significantly affecting losses from conduction within the bundle. This result yields two simple design guidelines for the choice of pitch length in a multi-level litz wire:

- An integer number of twists optimally minimizes proximity effect loss. Avoid using less than 1 twist of wire.
- For multilevel constructions, the proximity-effect magnetic fields originate from both within the litz wire as well as outside. Consequently, to minimize F in the two-level construction, the inner level should have integer twists relative to the outer level, and to minimize G, both levels should have integer twists relative to the global axis.

It becomes clear that the same underlying rule govern loss minimization in all cases, albeit in different coordinate systems, against magnetic fields flowing in different directions.

The overall losses are much higher than tolerable for > 1 MHz. While these results are included to illustrate conformity to theory, they are largely ignored for the purposes of litz wire design.

V. Experimental validation

In order to confirm that the simulation predictions conform to reality, we constructed a number of litz wires, of various strand wire gauges, pitch, number of strands, and number of levels. During this stage, it was discovered that the helical model in Section III-A is structurally unsound for more than three strands, and will tend to collapse into hexagonal packing under tension. Consequently, in order to ensure that the computational model matches the experimental specimen, a three-stranded litz wire construction was chosen.

First, a 66 cm long, three-stranded twisted bundle with a helical pitch of 1 ± 0.05 cm was constructed from AWG 32 wires, which have diameters of 202 μm, and insulation around 30 μm. This bundle was then twisted into a 19 cm long, 3×3 litz wire, with helical pitch set to 1 ± 0.04 cm in the opposite direction. The latter construction is shown with its computation model in Fig. 9. Terminal impedances were measured using an Agilent 4192A low-frequency impedance analyzer, with the wires laid in a zig-zag, serpentine fashion to minimize inductance and proximity effect loss. A resonant peaking characteristic was observed in both sets of measurements; 60 pF of parallel capacitance was estimated by least-squares fitting over a large set of data and removed accordingly. The analytical predictions were made using equation (5) from [10].

Both the numerical and the analytical methods produced excellent fits to measurements for the three stranded bundle
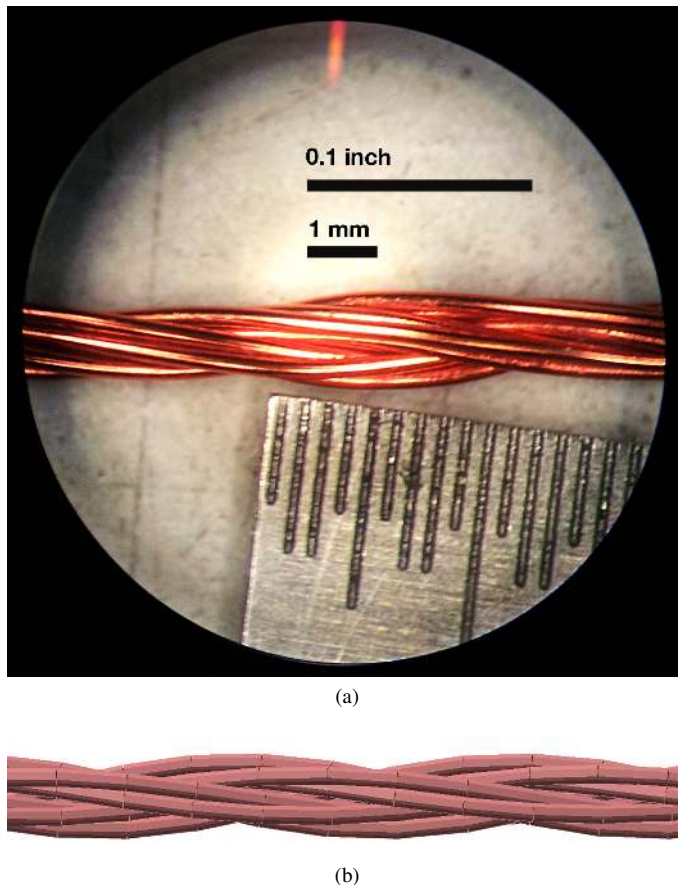

(a)

(b)

Figure 9: To-scale comparison of the computational model and the actual litz wire tested.

in Fig. 10a, particularly around the knee frequency of 100-300 kHz, which is the range of most practical interest for the designer. The numerical simulation accuracy degrades beyond this range. This is an expected result with the use of a coarse mesh in the conductor, following the discussion in Section II-B.

Results for the 3×3 wire are shown in Fig. 10b. The analytical solution significantly under-predicts the resistance of the wire, because it assumes an ideal litz construction, where the current density is perfectly identical within each strand. The numerical solution fits better in comparison, by avoiding this assumption and explicitly modeling the non-ideal wire construction. None-the-less, the fit is poorer than before. From Fig. 9, we see that the experimental specimen contains defects in its fabrication. In particular, the inner level was partially unwound, in an uncontrolled manner, by the twisting of the outer level. The physical differences between the computational model and the experimental wire sample may explain the discrepancy between the predictions and the measurements.

VI. Conclusions & Future Work

A characterization procedure is presented for the skin and proximity effect losses of realistic litz wire, based on a fast
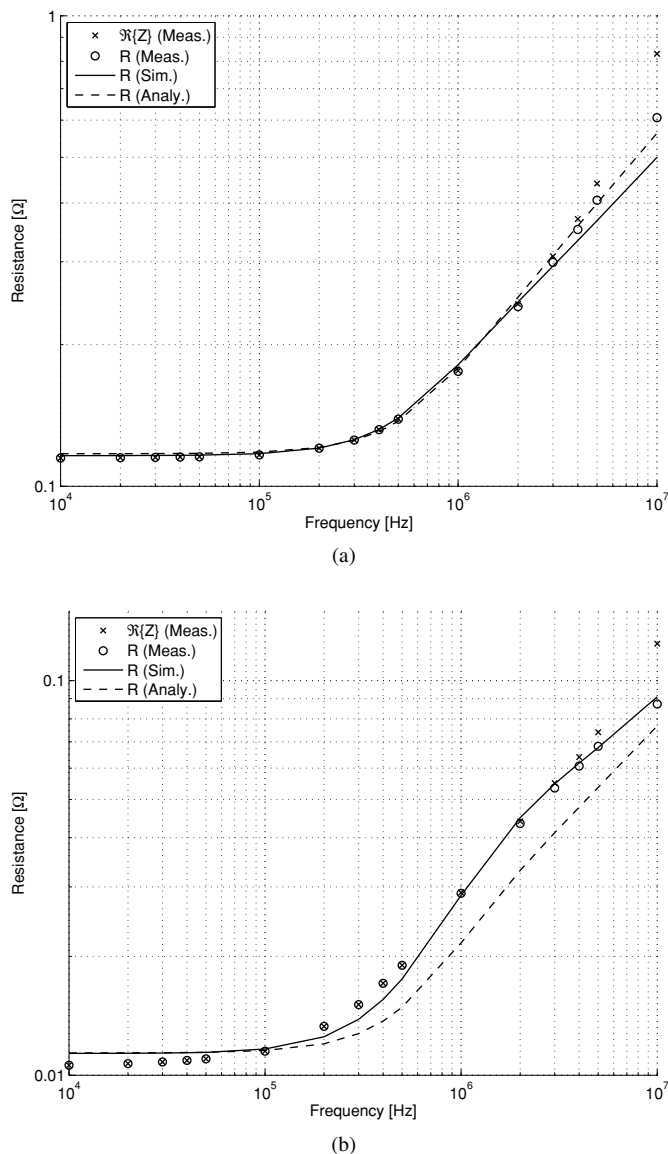
(a)

(b)

Figure 10: Measured vs predicted resistances for (a) a single strand of $3 \times$ AWG 32 gauge wire, and (b) a two-level litz wire constructed from $3 \times 3 \times$ AWG 32 gauge wire. Measured resistances obtained by removing contributions by 60 pF of parallel capacitance from $\Re\{Z\}$. Analytical solution taken from [10].

numerical simulation tool. To the best of our knowledge, this is the first systematic effort to characterize these loss mechanisms in non-ideal litz wire using a computational method. The procedure can be swept over a range of construction parameters, allowing optimization of the wire construction to be performed. The procedure is applied to a circular litz wire construction, and the predictions made are experimentally validated.

The experiences described in this paper confirm the capability of numerical methods to provide valuable insights into the construction of litz wire, and evidence for their

computational efficiency. However, the efficacy and predictive ability of the approach is also closely tied to the faithfulness of the computational model itself. Therefore, a natural extension to this work is to adapt numerical methods to increase the modeling accuracy of litz wire.

The full program and source code may be found at [18].

REFERENCES

[1] C. Sullivan, "Cost-constrained selection of strand diameter and number in a litz-wire transformer winding," *IEEE Transactions on Power Electronics*, vol. 16, no. 2, pp. 281–288, Mar. 2001.

[2] X. Tang and C. Sullivan, "Stranded wire with uninsulated strands as a low-cost alternative to litz wire," in *Proc. IEEE PESC'03*, vol. 1, 2003, pp. 289–295.

[3] H. Rossmanith, M. Doebroenti, M. Albach, and D. Exner, "Measurement and Characterization of High Frequency Losses in Nonideal Litz Wires," *IEEE Transactions on Power Electronics*, vol. 26, no. 11, pp. 3386–3394, Nov. 2011.

[4] P. Reddy, T. Jahns, and T. Bohn, "Transposition effects on bundle proximity losses in high-speed PM machines," in *Proc. IEEE ECCE'09*, Sep. 2009, pp. 1919–1926.

[5] C. Sullivan, "Optimal choice for number of strands in a litz-wire transformer winding," in *Proc. IEEE PESC'97*, vol. 1, 1997, pp. 28–35.

[6] J. Acero, R. Alonso, J. Burdio, L. Barragán, and D. Puyal, "Frequency-dependent resistance in litz-wire planar windings for domestic induction heating appliances," *IEEE Transactions on Power Electronics*, vol. 21, no. 4, pp. 856–866, 2006.

[7] R. Zhang, J. White, and J. Kassakian, "Fast simulation of complicated 3D structures above lossy magnetic media," *IEEE Transactions on Magnetics*, to be published.

[8] J. Ferreira, "Improved analytical modeling of conductive losses in magnetic components," *IEEE Transactions on Power Electronics*, vol. 9, no. 1, pp. 127–131, 1994.

[9] P. Dowell, "Effects of eddy currents in transformer windings," *Proceedings of the IEEE*, vol. 113, no. 8, pp. 1387–1394, 1966.

[10] J. Ferreira, "Analytical computation of AC resistance of round and rectangular litz wire windings," *Electric Power Applications, IEE Proceedings B*, vol. 139, no. 1, pp. 21–25, 1992.

[11] N. McLachlan, *Bessel functions for engineers*. Oxford: Clarendon Press, 1955.

[12] A. Ruehli, "Equivalent Circuit Models for Three-Dimensional Multiconductor Systems," *IEEE Transactions on Microwave Theory and Techniques*, vol. 22, no. 3, pp. 216–221, Mar. 1974.

[13] M. Kamon, M. Ttsuk, and J. White, "FASTHENRY: a multipole-accelerated 3-D inductance extraction program," *IEEE Transactions on Microwave Theory and Techniques*, vol. 42, no. 9, pp. 1750–1758, 1994.

[14] A. E. Ruehli, "Inductance Calculations in a Complex Integrated Circuit Environment," *IBM Journal of Research and Development*, vol. 16, no. 5, pp. 470–481, Sep. 1972.

[15] W. T. Weeks, L. L.-H. Wu, M. F. McAllister, and A. Singh, "Resistive and Inductive Skin Effect in Rectangular Conductors," *IBM Journal of Research and Development*, vol. 23, no. 6, pp. 652–660, Nov. 1979.

[16] C. Schuster, G. Leonhardt, and W. Fichtner, "Electromagnetic simulation of bonding wires and comparison with wide band measurements," *IEEE Transactions on Advanced Packaging*, vol. 23, no. 1, pp. 69–79, 2000.

[17] "Round Litz." [Online]. Available: http://newenglandwire.com/products/litz-and-formed-cables/round.aspx

[18] R. Y. Zhang, "Computation Codes." [Online]. Available: http://web.mit.edu/ryz/www